A Theoretical Modeling and Analysis of Communication via Heat Flow at Nanoscale

Deniz Kilinc, *Student Member, IEEE*, and Ozgur B. Akan, *Senior Member, IEEE*

***Abstract*—Nanonetworks constructed by interconnecting nanodevices using wireless communication allow the nanodevices to perform more complex functions by means of cooperation between them. For the first time in the literature, a novel and physically realizable nanoscale communication technique is introduced: Nanoscale Heat Communication (NHC) in which the heat transfer is used for communication at the nanoscale. The transmitted information is encoded in temperature signals using Magneto-Caloric Effect (MCE) which is the change in temperature of a magnetic material exposed to a varying magnetic field. Thermal energy emitted or absorbed by a transmitter nanodevice is subject to the laws of thermal diffusion which changes the temperature of the communication medium. The transmitted information is decoded by a receiver nanodevice that senses the temperature variations. Using information theoretical analysis, a closed-form expression for the channel capacity is obtained. According to the performance evaluation of the channel capacity, NHC provides a significantly higher capacity communication compared with the existing molecular communication techniques. Therefore, NHC stands as a promising solution to nanoscale communication between nanomachines based on its channel capacity performance, advantages, and possible applications for the emerging field of nanonetworks.**

***Index Terms*—Nanoscale heat communication, magneto-caloric effect, nanoscale communication.**

I. Introduction

NANOSCALE communication between nanodevices is a novel and interdisciplinary concept which includes nanotechnology, biotechnology, and communication technology [1]. The nanonetworks constructed by interconnecting nanodevices expand the capabilities of single nanodevices by means of cooperation between them [2]. The realization of the nanoscale communication can be achieved through electromagnetic, acoustic, or molecular communication [3], [4]. Although recently, Molecular Communication (MC) has been considered as a promising solution for the communication of nanodevices [5]–[7], there are several disadvantages of MC. For example, the limitation in the molecule storage of a nanodevice restricts the lifetime of a nanonetwork and makes MC impractical. In addition, refilling the molecule storage of a nanodevice is very challenging. Furthermore, in MC, the emission of the signal molecules in the communication medium may result in undesired accumulation of these molecules.

For the first time in the literature, we introduce a novel and radically different nanoscale communication concept: Nanoscale Heat Communication (NHC) in which the heat transfer is used for communication at the nanoscale. NHC is based on the diffusion of thermal energy. That is, the temperature of the transmitter nanodevice is modulated according to the transmitted information. Thermal energy emitted due to an increase in the temperature of the transmitter or absorbed due to a decrease in the temperature of the transmitter changes the temperature at the receiver location according to the laws of thermal diffusion. Then, the temperature variation at the receiver location is sensed by the receiver nanodevice using a thermal nanosensor. Although in [8], [9], the authors consider radiative exchange of heat between nanostructures, they consider only nanostructures that are in close proximity. Also, they do not propose and analyze a communication system. Therefore, our proposed nanoscale communication system is completely different than the existing studies.

The temperature modulation of the transmitter nanodevice is achieved by using Magneto-Caloric Effect (MCE) which is a well-known phenomenon defined as the change in temperature of magnetic materials exposed to a varying magnetic field [10]. We use MCE in NHC because it can be successfully implemented for temperature modulation, i.e., both increasing and decreasing temperature level, at the nanoscale. Therefore, using MCE instead of Joule heating to change the temperature is more advantageous because Joule heating cannot be used to decrease the temperature of the transmitter which is crucial for the proposed communication system [11].

The transmitter nanodevice can modulate the temperature of the nanoparticle to transmit the desired information by utilizing a nanosolenoid [12] to create a magnetic field and a magnetic nanoparticle. Recently, the production of carbon nanosolenoids have been successfully realized using carbon nanotubes (CNTs) [12]–[14]. In addition, the theoretical analyses of the CNT bundle-based inductors are presented in [15], [16]. CNTs bundle-based inductors have been proposed as a possible replacement for copper inductors due to their high conductivity and current carrying capabilities [17], [18].

Magnetic nanoparticles have been used for their ability to exhibit large MCE; e.g., the temperature of gadolinium (Gd) nanoparticles can be increased by 2 K at room temperature by applying a magnetic field having approximately 500 mT

Manuscript received March 27, 2014; revised July 21, 2014; accepted August 17, 2014. Date of publication August 28, 2014; date of current version October 17, 2014. This work was supported in part by the Turkish Scientific and Technical Research Council under grant #109E257, by the Turkish National Academy of Sciences Distinguished Young Scientist Award Program, and by IBM through IBM Faculty Award. The associate editor coordinating the review of this paper and approving it for publication was M. Pierobon.

The authors are with the Next-generation and Wireless Communications Laboratory (NWCL), Department of Electrical and Electronics Engineering, Koc University, Istanbul 34450, Turkey (e-mail: dkilinc@ku.edu.tr; akan@ku.edu.tr).

Color versions of one or more of the figures in this paper are available online at http://ieeexplore.ieee.org.

Digital Object Identifier 10.1109/TCOMM.2014.2353047

strength [19]. For instance, magnetic nanoparticles are utilized in an experimental cancer treatment called magnetic hyperthermia in which MCE is used to heat and kill a tumor [20]. Furthermore, according to the results revealed in [12], CNT-based nanosolenoids having a magnetic core with high permeability might generate a magnetic field with a strength on the order of hundreds of mT. Hence, MCE can be conveniently utilized in NHC to modulate the temperature of a magnetic nanoparticle. As a result, unlike the most of the existing nanoscale communication methods in the literature, NHC technique is physically realizable and hence, NHC can be experimentally validated.

NHC is based on the diffusion of thermal energy; thus, NHC and MC are similar because MC depends on the diffusion of molecules. However, NHC does not have the disadvantages of MC. In NHC, the electrical energy is converted to thermal energy. Therefore, in NHC, a nanobattery is enough to provide power required for the communication unlike MC. Recently, novel energy harvesting techniques have been proposed to recharge the energy stored in the nanobatteries [21]. For instance, an experimental study for a piezoelectric nanogenerator is shown in [22]. Thus, by using these techniques, it is possible to overcome the energy bottleneck of nanonetworks and to make their lifetime infinite. Furthermore, the speed of the diffusion is proportional to the diffusion coefficient. The diffusion coefficients of biological molecules range from 10^{-10} m^2/s to 10^{-11} m^2/s [23], [24]. On the other hand, the thermal diffusion constants of water and air at room temperature are 0.143×10^{-6} m^2/s and 1.9×10^{-5} m^2/s, respectively, which provides $\sim 10^5$ fold higher communication speeds to NHC compared with MC. Thus, NHC can be used for significantly higher data rates than the rates achieved by MC.

Unlike MC, binary bipolar encoding can be used in NHC. That is, the temperature of the transmitter nanodevice can be modulated according to the binary bipolar encoding using MCE. As a result, the expected temperature variation of the medium due to NHC becomes zero. However, in MC, the accumulation of the molecules in a closed medium is an inevitable result [25], which can also be an advantage [26]. Furthermore, NHC can take place in three states of the matter, i.e., solid, liquid, or gaseous, since the thermal diffusion occurs in these states. However, MC can be realized only in a liquid [23]. On the other hand, in MC, a transmitter nanodevice can emit specific type of molecules for the ligand-binding reception so that a receiver nanodevice can differentiate the molecules emitted by the transmitter from molecules in the communication medium [27], which can increase communication range of MC [28].

The device implementation of NHC is simple compared with MC since a nanodevice can become a transmitter by incorporating a nanosolenoid and a magnetic nanoparticle into the nanodevice and, similarly, a nanodevice can receive the transmitted temperature signals only by using a thermal nanosensor. Although the device implementation of MC is more complex than NHC, MC is a bioinspired method and hence it is a biocompatible nanoscale communication technique. Thus, it might be more troublesome to utilize NHC for intrabody applications compared to MC. That is, for intrabody applications, using MC might be more favorable than NHC. The summary of the comparison of NHC and MC is given in Table I. NHC stands as a promising solution to realize nanoscale communication between nanomachines based on its advantageous properties.

TABLE I
COMPARISON TABLE OF MOLECULAR COMMUNICATION AND NANOSCALE HEAT COMMUNICATION

Property	**MC**	**NHC**
Physical phenomenon	*Molecular diffusion*	*Thermal diffusion*
Lifetime	*Limited*	*Unlimited*
Data rate	*Low*	*High*
Communication Medium	*Liquid*	*Solid, liquid, gas*
Effect on medium	*Molecule accumulation*	*No total effect*
Communication distance	*Long range*	*Short range*
Device implementation	*Complex*	*Simple*
Intrabody implementation	*Biocompatible*	*Difficult*

The rest of the paper is organized as follows. In Section II, we explain the basic concepts of MCE and underline the governing physical laws and its mathematical formulations. In Section III, we describe the physical model of NHC and explain how each of the components in the communication model works. In Section IV, we perform an information theoretical analysis of NHC to determine the closed-form expression for the channel capacity and the signal-to-noise ratio (SNR). Section V presents numerical analyses of both the channel capacity and the SNR for NHC channel. Finally, Section VI concludes the paper.

II. THEORY OF MAGNETO-CALORIC EFFECT

Magneto-Caloric Effect (MCE) is defined as the response of magnetic materials to a varying magnetic field which manifests as a change in the entropy and temperature of the magnetic material [10]. MCE is an intrinsic property of all magnetic materials and is caused by the coupling of the magnetic sublattice[1] with the magnetic field [29]. In Fig. 1, the thermodynamics of MCE for a ferromagnet,[2] i.e., the entropy of the ferromagnetic material S with respect to the temperature T, for both zero magnetic field H_0 and a nonzero magnetic field H_1 is schematically illustrated. If the magnetic field H_1 is applied to the ferromagnet in an adiabatic process[3] in which the total entropy of the system remains constant, the temperature of the system increases due to MCE, which is called the adiabatic temperature change and denoted by ΔT_{ad}. The adiabatic temperature change can be visualized as the temperature difference between (S_0, T_0) and (S_0, T_1) points shown in Fig. 1 by the horizontal arrow, i.e., $\Delta T_{ad} = T_1 - T_0$.

MCE can also be expressed by means of the entropy change, denoted by ΔS, when the magnetic field H_1 is applied to the ferromagnet in an isothermal process.[4] Similar to the isothermal compression of a gaseous, the isothermal magnetization of a

[1]Magnetic sublattice is a system of identical magnetic atoms or ions positioned periodically in space, with magnetic moments of the same magnitude and direction.

[2]A material is a ferromagnet if all of its magnetic ions add a positive contribution to the net magnetization.

[3]An adiabatic process is defined as a process occurring without input or output of heat within a system, i.e., the system is thermodynamically isolated. Therefore, by the second law of thermodynamics, in an adiabatic process the entropy of the system does not change.

[4]An isothermal process is defined as a process in which the temperature remains constant. In an isothermal process, there is heat transfer between the system and the surroundings which causes the entropy of the system change by the second law of thermodynamics.

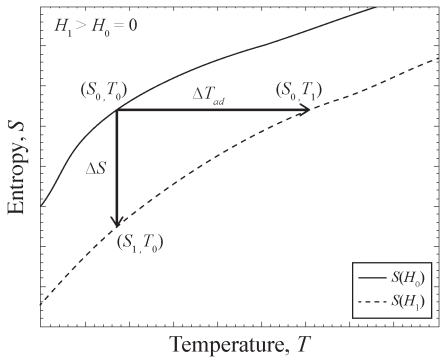

Fig. 1. The schematic demonstration of the entropy of the ferromagnetic material with respect to the temperature for zero magnetic field H_0 and a nonzero magnetic field H_1 [29].

soft ferromagnet or a paramagnet reduces the entropy of the material and the isothermal demagnetization restores the zero magnetic field entropy of the material similar to the isothermal expansion of a gaseous. The isothermal entropy change is represented by the difference between (S_0, T_0) and (S_1, T_0) points illustrated in Fig. 1 by the vertical arrow, i.e., $\Delta S = S_0 - S_1$.

The isothermal entropy change ΔS and the adiabatic temperature change ΔT_{ad} represent two quantitative characteristics of MCE. ΔS and ΔT_{ad} are derived using one of the fundamental Maxwell's relations [30]

$$\left(\frac{\partial S(T,H)}{\partial H}\right)_T = \left(\frac{\partial M(T,H)}{\partial T}\right)_H, \tag{1}$$

where $S(T,H)$ is the total entropy, $M(T,H)$ is the magnetization, H is the magnetic field strength, T is the absolute temperature and the subscript outside the parentheses indicates which variable is being held constant during differentiation. For an adiabatic process, the integration of the expression given in (1) yields [30]

$$\Delta T_{ad} = -\int_{H_i}^{H_f} \frac{T}{C(T,H)_H}\left(\frac{\partial M(T,H)}{\partial T}\right)_H dH, \tag{2}$$

where H_i and H_f are the initial and final magnetic fields, respectively, applied to the magnetic material, and $C(T,H)_H$ is the heat capacity of the magnetic material at constant magnetic field as indicated by the subscript H. Thus, the adiabatic temperature change is proportional to the absolute temperature, to the magnetic field change and to the derivative of magnetization with respect to temperature at constant magnetic field; it is inversely proportional to the heat capacity.

III. Physical Model of Nanoscale Heat Communication

NHC model consists of a transmitter nanodevice (TN), a receiver nanodevice (RN), a thermal diffusion channel between TN and RN, and a noise caused by the stochastic fluctuations in the temperature at the output of the channel. In this section, we introduce NHC model by describing how each of the components in the communication model works.

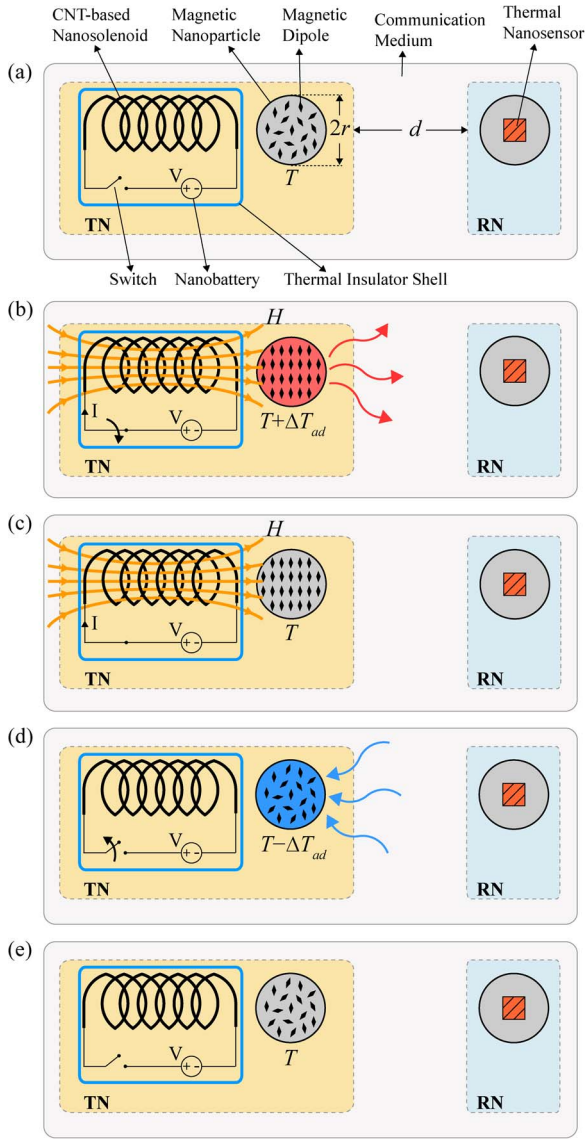

Fig. 2. NHC model and the temperature encoding mechanism with binary bipolar coding.

A. Transmitter

TN uses the binary bipolar encoding for the transmission of the binary information bits $\{a_j\}$. To transmit the information, the temperature of TN is modulated according to the bipolar encoded signal. That is, a binary bit 0 is transmitted by a zero temperature change and a binary bit 1 is transmitted alternately by a positive temperature change and a negative temperature change with the same magnitude. The communication takes place in a 3D medium having a significantly larger extent than the size of nanodevices. Furthermore, the communication medium can be solid, liquid, or gaseous.

NHC with bipolar encoding is achieved by the utilization of MCE in TN. MCE is used in NHC since it can be successfully implemented to modulate the temperature at the nanoscale. Fig. 2(a) shows the simplified model of TN. TN includes a CNT-based nanosolenoid, a thermal insulator shell, a spherical magnetic nanoparticle, a nanobattery, and a switch. The CNT-based nanosolenoid is used to create the desired magnetic field

and change the temperature of the magnetic nanoparticle by means of MCE. Since a copper nanosolenoid has a significantly large resistance and low quality factor due to nanoscale dimensions of copper wires, we use a CNT-based nanosolenoid in TN for NHC. CNT-based nanosolenoids have extremely high conductivity and current carrying capabilities [17], [18]. Thus, Joule heating in the CNT-based nanosolenoid is significantly lower compared with a copper nanosolenoid. We also assume that the nanosolenoid is enclosed by a thermal insulator shell to prevent Joule heating from interfering with the temperature signals transmitted by TN. The switch is controlled by a controller circuit which is also encapsulated by the insulator which is not shown in Fig. 2.

The transmission process in NHC is described as follows:

a) Initially, the switch is open and there is no current flowing through the nanosolenoid; thus, there is no magnetic field created by the nanosolenoid as shown in Fig. 2(a). The temperature of the magnetic nanoparticle is the same as the temperature of the medium, denoted by T, i.e., the system is in thermal equilibrium.
b) Then, if the next information bit to be transmitted is a binary bit 0, the switch remains open and the thermal equilibrium condition is sustained because the binary bit 0 is transmitted by a zero temperature change. However, if the next information bit to be transmitted is a binary bit 1, the switch is closed instantaneously which causes a current flow through the nanosolenoid; thus, a magnetic field H is created by the nanosolenoid as illustrated in Fig. 2(b). Since the magnetic field H is applied instantaneously to the magnetic nanoparticle, the process of applying the magnetic field can be approximated as an adiabatic process. Thus, the temperature of the nanoparticle increases by ΔT_{ad} due to MCE. Then, heat flows from the nanoparticle to the communication medium due to the temperature difference. For example, the temperature of Gd nanoparticles increase by 2 K by applying a magnetic field having 500 mT strength at room temperature [19]. With the advances in nanotechnology, CNT-based nanosolenoids having a magnetic core with high permeability can generate a magnetic field with a strength on the order of hundreds of mT [12]. Thus, MCE can be conveniently used in NHC to modulate the temperature of a magnetic nanoparticle.
c) In NHC, the temperature of the magnetic nanoparticle is modulated according to the binary bipolar encoding; then, the expected value of the temperature change of the medium is zero. Furthermore, since the extent of the communication medium is assumed to be significantly larger compared with the size of the magnetic nanoparticle, the heat capacity of the communication medium is also significantly larger than the heat capacity of the nanoparticle. For instance, 1 L of water at room temperature $T = 300$ K has a heat capacity $C_V = 4140$ J/K and a nanoparticle has a heat capacity on the order of 10^{-18} J/K [31]. Thus, the steady state temperature change of the communication medium caused by NHC is negligible compared with the temperature of the medium T and hence T can be assumed to be unchanged. Then, the magnetic nanoparticle returns to its initial temperature T after the thermal equilibrium is reached as shown in Fig. 2(c).
d) After transmitting the binary bit 1, if the next information bit to be transmitted is a binary bit 0, the switch remains closed and the magnetic field H is held constant. However, if the next information bit to be transmitted is a binary bit 1, the switch is opened instantaneously, which cuts off the current flowing through the nanosolenoid; thus, the magnetic field H disappears as shown in Fig. 2(d). Since the magnetic field H that is applied to the magnetic nanoparticle instantaneously vanishes, the process of the removal of the magnetic field can be approximated as an adiabatic process. Hence, the temperature of the nanoparticle decreases by ΔT_{ad} due to MCE. Then, heat flows from the medium to the nanoparticle because of the temperature difference.
e) The heat capacity of the communication medium is large enough that the temperature of the medium T is assumed to be unchanged (see item (c) above) and hence the temperature of the nanoparticle returns to its initial value T after the thermal equilibrium is reached as shown in Fig. 2(e). That is, the system reaches its initial condition (see item (a) above). Therefore, the information transmission process continues from item (a) in a cyclic manner.

When the switch is closed instantaneously, the temperature of the magnetic nanoparticle adiabatically increases by ΔT_{ad}. At the end of the adiabatic process, the temperature of the magnetic nanoparticle changes according to the thermal diffusion. In other words, the initial condition for the temperature of the magnetic nanoparticle is $T+\Delta T_{ad}$ before the thermal diffusion takes place. Thus, the adiabatic temperature change can be modeled as an impulse function with a magnitude ΔT_{ad}. Furthermore, the radius of the spherical magnetic nanoparticle is considered negligible with respect to the distance between the TN and the RN; that is, $r \ll d$. Therefore, the magnetic nanoparticle is approximated as a point source emitting desired temperature signals at the location $(x=0, y=0, z=0)$. Finally, the temperature variation of the magnetic nanoparticle is expressed as

$$s(x, y, z, t) = \Delta T_{ad}\delta(x, y, z, t). \tag{3}$$

According to the information transmission process described above, the total temperature variation of the nanoparticle located in TN is given by

$$s_T(x, y, z, t) = \sum_{j=-\infty}^{\infty} b_j s(x, y, z, t - jT_s), \tag{4}$$

where $\{b_j\}$ is the bipolar encoded sequence of the binary information sequence $\{a_j\}$ and T_s is the signaling interval. The block diagram representation of the transmitter and channel can be seen in Fig. 3(a).

B. Signal Propagation

The transmission of the information from TN to RN is achieved by the propagation of the temperature signals transmitted by TN. The temperature signals propagate from TN to

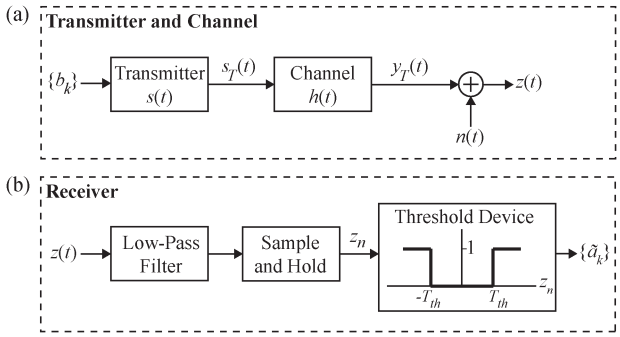

Fig. 3. The block diagram representation of (a) transmitter and channel, and (b) receiver for NHC model.

RN only by means of the laws of conductive heat transfer, i.e., thermal diffusion. To derive the impulse response of the thermal diffusion channel, we use the heat equation which describes the variation in temperature in a given region over time [32]. The heat equation is given by

$$\frac{\partial u(x,y,z,t)}{\partial t} = \alpha \nabla^2 u(x,y,z,t), \tag{5}$$

where $u(x,y,z,t)$ is the temperature of the point (x,y,z) at time t, $\nabla^2 u(x,y,z,t)$ is the sum of the 3D spatial second derivatives of $u(x,y,z,t)$, and α is the thermal diffusivity of the medium. The usual heat equation is valid for the heat transfer in a system with nanoparticles in the absence of phase transformations [33]. The impulse response of the thermal diffusion channel can be found by solving (5) for a point heat source with an initial condition given by $u(x,y,z,t=0) = \delta(x,y,z)$. The response of (5) to this initial condition yields the impulse response of the thermal diffusion channel, denoted by $h(t)$, and it is is given as follows

$$h(t) = \frac{V}{(4\pi t\alpha)^{3/2}} \exp\left(-\frac{|d|^2}{4t\alpha}\right),\ t>0, \tag{6}$$

where V is the volume of the magnetic nanoparticle, i.e., $V=(4/3)\pi r^3$, $|d|$ is the Euclidean distance between RN and TN, i.e., $|d| = \sqrt{(x_R)^2+(y_R)^2+(z_R)^2}$, and (x_R, y_R, z_R) is the location of RN in 3D Cartesian coordinate system. To have a compact notation, we drop (x,y,z) term in $h(x,y,z,t)$ because TN and RN are located at fixed positions. Since the thermal diffusivity constant is assumed to be time-invariant, NHC channel is time-invariant.

The temperature change at the location of RN caused by the temperature variation of the magnetic nanoparticle can be obtained as

$$y(t) = s(t) * h(t) = \frac{\Delta T_{ad} V}{(4\pi t\alpha)^{3/2}} \exp\left(-\frac{|d|^2}{4t\alpha}\right),\ t>0, \tag{7}$$

where $*$ denotes the convolution operator. The total temperature change at the location of RN is

$$y_T(t) = \sum_{j=-\infty}^{\infty} b_j y(t - jT_s). \tag{8}$$

C. Noise

At the output of the thermal diffusion channel, a noise is added to the total temperature variation signal $y_T(x,t)$. The additive noise, denoted by $n(t)$, is a result of thermal fluctuations which are random deviations of a system from its equilibrium. Since thermal fluctuations arise due to random vibrations or random rotations of molecules, the stochastic behavior of the thermal fluctuations is described by a Gaussian distribution based on the central limit theorem [34]. The power spectral density[5] (PSD) of the thermal fluctuations generated by an additive Gaussian noise process is given as [35]

$$S_n(f) = \frac{k_B T^2}{C_V}, \tag{9}$$

where T is the temperature of the communication medium, C_V is the heat capacity of the medium at constant volume, and k_B is Boltzmann constant. Since in NHC, the temperature of the magnetic nanoparticle is modulated according to the binary bipolar encoding, the expected value of the temperature change of the medium is zero. Furthermore, since the heat capacity of the communication medium is assumed to be significanlty larger than the heat capacity of the magnetic nanoparticle, the steady state temperature change of the medium is considered negligibly small compared with the temperature of the medium T. For example, 1 L of water at room temperature $T=300$ K has a heat capacity $C_V=4140$ J/K and a nanoparticle has a heat capacity on the order of 10^{-18} J/K [35]. Therefore, the temperature of the medium T and the PSD of the noise are assumed to be constant. Consequently, based on the aforementioned assumptions, the additive noise in NHC can be modeled as an additive white Gaussian noise (AWGN) with a PSD expressed in (9).

D. Receiver

RN is located at a distance d from TN and the total instantaneous temperature variation at the receiver location is

$$z(t) = y_T(t) + n(t). \tag{10}$$

RN includes a thermal nanosensor to detect the temperature signals transmitted by TN. For example, a cantilever-based thermal nanosensor can have a sensitivity of $\sim 10^{-5}$ K [36] and a sensor based on coupled microwave resonators can have $\sim 10^{-9}$ K temperature sensitivity [37]. To increase the signal-to-noise ratio (SNR) of the received electrical signals, the power of the noise is limited by a low pass filter (LPF) with unity gain before sampling the temperature. For instance, to filter temperature signals, phonon[6] filters can be used to prevent a spectral band of phonons from propagating [38]. The bandwidth of the LPF, denoted by B, is chosen to satisfy $B \geq 2/T_s$ so that the bipolar signaling wave shape is preserved at the filter output, yet the noise power is reduced by the filter [39]. It is assumed that RN samples the output of the LPF with a sampling time T_s which is equal to the signaling interval of TN, and converts the sampled signals to electrical signals. Thus, assuming the

[5]Power spectral density of a signal describes how the power of the signal is distributed over different frequencies

[6]Phonon is the central thermal energy carrier for conductive heat transfer.

detection is coherent and there is no intersymbol interference (ISI), the temperature variation signal sampled by RN is

$$z_k = \Delta T_{\max} b_k + n_k, \tag{11}$$

where $z_k = z(kT_s)$, $n_k = n(kT_s)$, and $\Delta T_{\max}$ is defined as the maximum temperature change at the receiver location and it is given by

$$\Delta T_{\max} = \max_t y(t) = \frac{\Delta T_{ad} V}{\left(\frac{2}{3}\pi e d^2\right)^{3/2}}. \tag{12}$$

The delay required for the temperature of the reception space reaches its maximum value, denoted by $t_{\max}$, is given as

$$t_{\max} = \arg\max_t y(t) = \frac{d^2}{6\alpha}. \tag{13}$$

The output of the sample and hold device is passed through a threshold device. The output of the threshold device gives the detected bits that are transmitted by TN. If $|z_n| > T_{th}$, the output of the threshold device is 1, otherwise 0 where T_{th} is the threshold temperature. To have a negligible ISI, the sampling time T_s should be large enough, i.e., $T_s \gg t_{\max}$. The block diagram of the receiver can be seen in Fig. 3(b).

IV. An Information Theoretical Analysis of Nanoscale Heat Communication

In this section, we present an information theoretical analysis of NHC. According to the communication model described above, NHC channel is time-invariant, has an additive white Gaussian noise (AWGN), and utilizes the binary bipolar signaling for the information transmission. To characterize the channel of NHC, first, we derive the information transmission probabilities of the channel.

Since the channel noise is AWGN, it is a zero-mean wide-sense stationary Gaussian process. We know that for a Gaussian process at the input, the output of the linear processor is also a Gaussian process. Therefore, the noise sample at the output of the sampler device is a zero mean Gaussian random variable and the total output sample z_n is a Gaussian random variable whose mean value depends on the transmitted bipolar information bit b_n as in (11). That is, $\{z_n|+1 \text{ sent}\} \sim \mathcal{N}(\Delta T_{\max}, \sigma_0^2)$, $\{z_n|-1 \text{ sent}\} \sim \mathcal{N}(-\Delta T_{\max}, \sigma_0^2)$, $\{z_n|0 \text{ sent}\} \sim \mathcal{N}(0, \sigma_0^2)$ where σ_0^2 is the variance of the noise samples and it is equal to the average received noise power, denoted by $\overline{P}_n$, i.e., $\sigma_0^2 = \overline{P}_n$. The power of the noise is limited by the low-pass filter (LPF) before sampling the temperature; hence, the average received noise power $\overline{P}_n$ is given by

$$\overline{P}_n = \int_{-B}^{B} S_n(f) df = \frac{2Bk_B T^2}{C_V}. \tag{14}$$

If the threshold of the threshold device is $T_{th} = \Delta T_{\max}/2$, then, the probability of erroneous transmission of bit 1 is

$$\begin{aligned} q &= \frac{1}{2}\Pr(0 \text{ received}|+1 \text{ sent}) + \frac{1}{2}\Pr(0 \text{ received}|-1 \text{ sent}) \\ &= Q\left(\sqrt{\frac{\Delta T_{\max}^2}{4\overline{P}_n}}\right) - Q\left(\sqrt{\frac{9\Delta T_{\max}^2}{4\overline{P}_n}}\right) \end{aligned} \tag{15}$$

where $Q(\cdot)$ is the Q-function. The probability of erroneous transmission of bit 0 is

$$p = \Pr(1 \text{ received}|0 \text{ sent}) = 2Q\left(\sqrt{\frac{\Delta T_{\max}^2}{4\overline{P}_n}}\right). \tag{16}$$

Since $p \neq q$, NHC channel exhibits binary asymmetric channel (BAC) characteristics.

Assume that X is the transmitted bit by TN and Y is the received bit by RN. Then, we assume that TN transmits bit 1 with a probability P_T, i.e.,

$$P_X(x) = \begin{cases} P_T, & \text{if x=1} \\ 1 - P_T, & \text{if x=0.} \end{cases} \tag{17}$$

Using (17), the joint probability distribution of X and Y, denoted by $P_{XY}(x, y)$, is

$$P_{XY}(x,y) = \begin{cases} (1-p)(1-P_T), & \text{if } (x=0, y=0) \\ p(1-P_T), & \text{if } (x=0, y=1) \\ qP_T, & \text{if } (x=1, y=0) \\ (1-q)P_T, & \text{if } (x=1, y=1). \end{cases} \tag{18}$$

The joint distribution $P_{XY}(x, y)$ expresses the probability of that the observed output symbol is y and the transmitted symbol is x. The mutual information between X and Y denoted by $I(X;Y)$ is given in [40] as follows

$$I(X;Y) = \sum_{x,y} P_{XY}(x,y) \log_2 \frac{P_{XY}(x,y)}{P_X(x) P_Y(y)}, \tag{19}$$

where $P_Y(y)$ is the probability distribution of Y. It is straightforward to obtain $P_Y(y)$ using the joint distribution $P_{XY}(x, y)$. NHC channel capacity, denoted by C, is the maximum value of the mutual information [40] and the channel capacity C is found as follows

$$\begin{aligned} C = \max_{P(x)} I(X;Y) &= \frac{(1-p)H(q) - qH(1-p)}{q+p-1} \\ &\quad + \log_2\left(1 + 2^{\frac{H(1-p)-H(q)}{q+p-1}}\right) \end{aligned} \tag{20}$$

where $H(\cdot)$ is the binary entropy function defined as $H(q) = -q\log_2 q - (1-q)\log_2(1-q)$. Furthermore, the operational channel capacity in bits/sec (bps) is given as

$$C_{op} = \frac{C}{T_s}, \tag{21}$$

where T_s is the signaling time of NHC.

To derive an expression for the average received signal power, we start with the general expression for the PSD of the digital signal in (8), which is given in [39] as

$$S_y(f) = \frac{|Y(f)|^2}{T_s} \sum_{k=-\infty}^{\infty} R_k e^{j2\pi f k T_s}, \tag{22}$$

where R_k is the autocorrelation function of the bipolar encoded data, which is given as $R_k = \mathrm{E}[b_j b_{j+k}]$, and $Y(f)$ is the

Fourier Transform of $y(t)$ given by

$$Y(f) = \frac{\Delta T_{ad} V \exp\left(-d\sqrt{\frac{\pi|f|}{\alpha}}\right)}{4\alpha\pi d|f|} \times \left[|f|\cos\left(d\sqrt{\frac{\pi|f|}{\alpha}}\right) - jf\sin\left(d\sqrt{\frac{\pi|f|}{\alpha}}\right)\right] \quad (23)$$

Although the capacity achieving input distribution is not uniformly distributed, to simplify the mathematical analysis, we consider a transmitted binary information sequence $\{a_k\}$ in which 0's and 1's are equally likely, i.e., $\Pr(a_k=0)=\Pr(b_k=0)=1/2$ and $\Pr(a_k=1)=\Pr(b_k=\pm 1)=1/2$. Thus, the autocorrelation function for the bipolar encoded data is simply given by

$$R_k = \begin{cases} 1/2, & k=0 \\ -1/4, & |k|=1 \\ 0, & |k|\geq 2. \end{cases} \quad (24)$$

Then, the summation term in (22) becomes $\sum_{k=-\infty}^{\infty} R_k e^{j2\pi f k T_s} = \sin^2(\pi f T_s)$. Since the received signal is passed through the LPF, the average received signal power, denoted by $\overline{P}_s$, is given by

$$\overline{P}_s = \int_{-B}^{B} S_y(f)df = \frac{\Delta T_{ad}^2 V^2}{16 T_s \alpha^2 d^2 \pi^2} \int_{-B}^{B} \exp\left(-2d^2\sqrt{\frac{\pi|f|}{\alpha}}\right)\sin^2(\pi f T_s)df. \quad (25)$$

Therefore, the received signal-to-noise ratio (SNR) for NHC is found as follows

$$\text{SNR} = \frac{\overline{P}_s}{\overline{P}_n}, \quad (26)$$

where $\overline{P}_n$ and $\overline{P}_s$ are given in (14) and (25), respectively.

V. Performance Evaluation

In this section, we present the performance analysis of the signal-to-noise ratio (SNR) in (26) and the channel capacity in (20) and (21). In the numerical analyses, we show how the SNR and channel capacity of NHC vary according to several parameters namely the adiabatic temperature change, the thermal diffusivity constant, and the distance between TN and RN. The results of the numerical analyses are used to determine the appropriate configuration of NHC parameters to achieve high channel capacity.

The analyses are carried out with a single TN and a single RN configuration as described in Section III. For the analysis, the radius of the magnetic nanoparticle is $r = 5$ nm which is a typical nanoparticle radius size [41]. Since $T_s \gg t_{\max}$ condition should be satisfied to have a negligible ISI, we assume $T_s = 10t_{\max}$. As we state in Section III, if the condition $B \geq 2/T_s$ is fulfilled, the received signal shape at the output of the low-pass filter (LPF) is not distorted. Then, we set $B = 2/T_s$. The Boltzmann constant is $k_B = 1.38 \times 10^{-23}$ J/K. The communication is assumed to take place at room temperature, i.e., $T = 300$ K. Since nanodevices can be used in many different environments and NHC can take place in three states of the matter, i.e. solid, liquid, or gaseous, the communication medium for NHC depends on the application for which nanodevices are used. For the numerical analyses, we consider the communication medium as water with 1 L volume. The constant volume molar heat capacity of water at 300 K is 74.53 J/mol · K [31]. Thus, since the molar mass of water is 18 g, the heat capacity of the medium is found as $C_V = 74.53 \cdot (1000\text{ g}/18\text{ g})$ J/K $= 4.14 \times 10^3$ J/K. The thermal diffusivity of the water at 300 K is $\alpha = 1.43 \times 10^{-7}\text{m}^2/\text{s}$ [42]. The numerical analyses are performed using MATLAB.

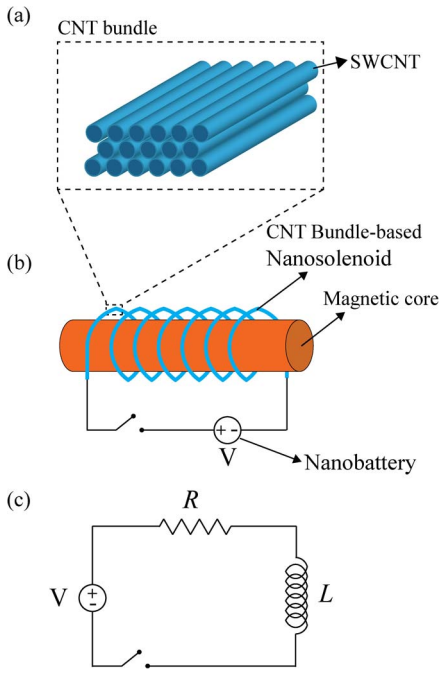

Fig. 4. The power consumption analysis of NHC. (a) The enlarged view of a CNT bundle. (b) The schematic representation of a CNT bundle-based nanosolenoid. (c) The equivalent circuit model.

A. Power Consumption Analysis

In this subsection, we analyze the power consumption of the TN for communication between TN and RN. We consider a CNT bundle-based nanosolenoid with a magnetic core to be able to generate the required magnetic field for NHC. CNT bundles, which form a CNT bundle-based nanosolenoid, are composed of Single-Walled CNTs (SWCNTs) as seen in Fig. 4(a). The schematic representation of a CNT bundle-based nanosolenoid and magnetic field generation system is shown in Fig. 4(b). The equivalent circuit model of the magnetic field generator is shown in Fig. 4(c).

To accurately characterize the resistance of a CNT bundle-based nanosolenoid, we adopt the equivalent conductivity model of CNT bundles presented in [15]. The equivalent conductivity model is an efficient and accurate approximation of the magnetic inductance of the discrete SWCNTs with a single conductor which has the same dimensions as the CNT bundle. Both the magnetic inductance and the ohmic resistance characteristics of the CNT bundle are captured by adjusting

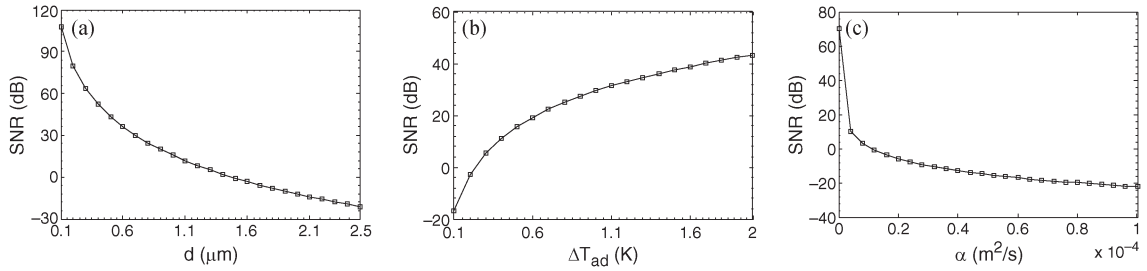

Fig. 5. The numerical analysis results performed over the SNR in dB with respect to the (a) communication distance d (for $\Delta T_{ad} = 2$ K, $\alpha = 1.43 \times 10^{-7}$ m^2/s), (b) adiabatic temperature change ΔT_{ad} (for $d = 500$ nm, $\alpha = 1.43 \times 10^{-7}$ m^2/s), and (c) thermal diffusivity constant α (for $d = 500$ nm, $\Delta T_{ad} = 2$ K).

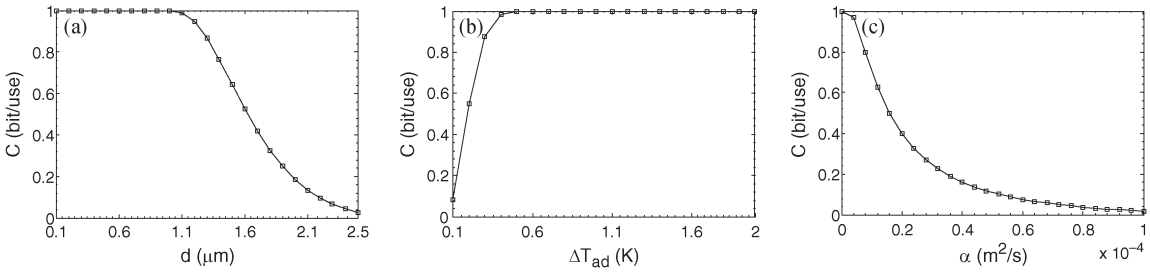

Fig. 6. The numerical analysis results performed over the channel capacity C in bit/use with respect to (a) the communication distance d (for $\Delta T_{ad} = 2$ K, $\alpha = 1.43 \times 10^{-7}$ m^2/s), (b) the adiabatic temperature change ΔT_{ad} (for $d = 500$ nm, $\alpha = 1.43 \times 10^{-7}$ m^2/s), and (c) the thermal diffusivity constant α (for $d = 500$ nm, $\Delta T_{ad} = 2$ K).

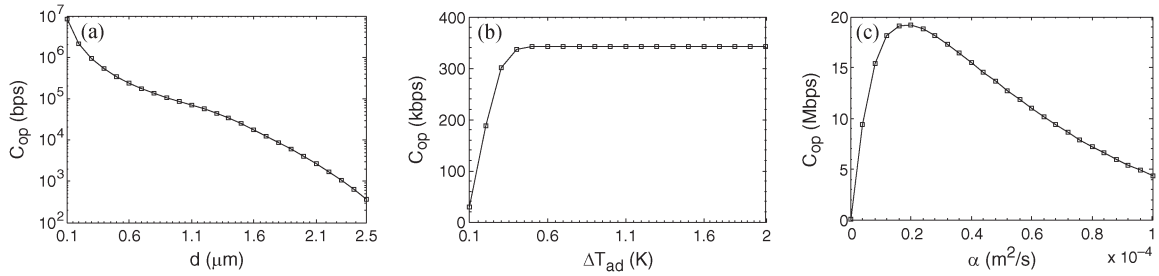

Fig. 7. The numerical analysis results performed over the channel capacity C_{op} in bps with respect to (a) the communication distance d (for $\Delta T_{ad} = 2$ K, $\alpha = 1.43 \times 10^{-7}$ m^2/s), (b) the adiabatic temperature change ΔT_{ad} (for $d = 500$ nm, $\alpha = 1.43 \times 10^{-7}$ m^2/s), and (c) the thermal diffusivity constant α (for $d = 500$ nm, $\Delta T_{ad} = 2$ K).

the resistivity of the single conductor to obtain a new effective resistivity, denoted by ρ_{eff}, which is given by $\rho_{\text{eff}} = \rho_c d_c^2 / P_m (1 - \lfloor 0.5 \lfloor t_s/d_c \rfloor \rfloor d_c^2 / w_s t_s)$ where ρ_c is the ohmic resistivity of an individual nanotube, d_c is the diameter of a SWCNT, P_m is the probability that a given SWCNT in the bundle is metallic, w_s and t_s are the width and thickness of the CNT bundle, respectively. Then, the resistance R of the nanosolenoid is given by $R = \rho_{\text{eff}} 2\pi r_s N / w_s t_S$ where r_s is the radius of the nanosolenoid. The generated magnetic field is $B = \mu_0 \mu_r N I / l_s$ where μ_0 is the magnetic permeability of free space, μ_r is the relative permeability of the magnetic core, N is the number of turns, I is the current passing through the nanosolenoid, and l_s is the length of the nanosolenoid.

For the power consumption analysis, we assume that $w_s = 4$ nm and $t_s = 4$ nm, $r_s = 25$ nm, $l_s = 100$ nm, $N = 1000$ turns, $\mu_r = 20000$. The diameter and resistivity of a SWCNT are given by $d_c = 1$ nm and $\rho_c = 10^{-8}\,\Omega$m, respectively [15]. In addition, we consider the probability that a given SWCNT in the bundle is metallic as $P_m = 10^{-16}$. To have $\Delta T_{ad} = 2$ K, we need to generate a magnetic field $B = 0.5$ T [19] and hence we need a current $I = 1.98$ nA passing through the nanosolenoid which have a resistance $R = 0.45\,\text{k}\Omega$. Therefore, the power consumption of the magnetic field generator circuit is $P_{\text{consumed}} = I^2 R = 1.76$ fW. In [22], it is shown that a piezoelectric nanogenerator can produce an average power density of $2.8\ \text{mWcm}^{-3}$. Therefore, a piezoelectric nanogenerator having a cubic shape with an edge length of 900 nm can generate a power of $P_{\text{battery}} = 2.04$ fW which is enough to create a magnetic field $B = 0.5$ T.

B. Effect of Communication Distance

In the second analysis, we investigate the effect of the communication distance d on the SNR and the channel capacity of NHC. In this part of the analysis, the adiabatic temperature change and the thermal diffusivity constant are kept unchanged at $\Delta T_{ad} = 2$ K and $\alpha = 1.43 \times 10^{-7}$ m^2/s, respectively. The SNR variation with respect to the communication distance d is illustrated in Fig. 5(a). The SNR decreases with an increase in d because as the communication distance increases, the received power of the temperature signal $\overline{P}_s$ decreases, which can be seen in (25). For example, SNR $= 107.7$ dB at $d = 100$ nm and SNR $= -21.1$ dB at $d = 2.5$ μm.

In Fig. 6(a), the variation of the channel capacity C in bit/use with respect to the communication distance d is shown. For short communication distances, since the SNR is too high as seen in Fig. 5(a), the effect of the noise on the information transmission is negligible; that is, the erroneous transmission probabilities p and q are too small. For instance, for a communication distance $d < 1.0$ μm, the SNR > 15 dB and the channel capacity has its maximum value $C = 1.0$ bit/use. On the other hand, for long communication distances, since the SNR decreases and becomes negative, the effect of the noise turns out significant and reduces the channel capacity. For example, for $d > 1.0$ μm, C decreases and becomes $C = 0.03$ bit/use at $d = 2.5$ μm as shown in Fig. 6(a).

The channel capacity $C_{op} = C/T_s$ in bps changes with respect to the communication distance d as shown in Fig. 7(a). Note that, the variations of the channel capacity in bit/use and bps with respect to d are different because substituting $T_s = 10t_{\max}$ and (13) in (21) yields $C_{op} = 0.6\alpha C/d^2$. Thus, the channel capacity C_{op} in bps decreases with an increase in d as seen in Fig. 7(a), although the channel capacity in bit/use is constant and $C = 1.0$ bit/use for $d < 1.0$ μm. For $d > 1.0$ μm, C in bit/use also decreases as d increases, which causes the C_{op} in bps to decrease faster with respect to d. For example, the channel capacity is $C_{op} = 8.58$ Mbps at $d = 100$ nm and it becomes $C_{op} = 0.37$ kbps at $d = 2.5$ μm. Therefore, we can say that NHC can provide very high communication rates over a long communication range compared with existing nanoscale communication techniques in the literature.

C. Effect of Adiabatic Temperature Change

In this analysis, we investigate the effect of the adiabatic temperature change ΔT_{ad} on the SNR and the channel capacity. The communication distance and the thermal diffusivity constant are kept unchanged at $d = 500$ nm and $\alpha = 1.43 \times 10^{-7}$ m^2/s, respectively, during this part of the analysis. The SNR variation with respect to the adiabatic temperature change ΔT_{ad} is demonstrated in Fig. 5(b). The SNR increases with an increase in ΔT_{ad}, which is an expected result because as ΔT_{ad} increases, the received power of the temperature signal $\overline{P}_s$ increases as seen in (25).

The channel capacity C in bit/use with respect to the adiabatic temperature change ΔT_{ad} is shown in Fig. 6(b). For a small adiabatic temperature change, since the SNR is too low as seen in Fig. 5(b), the effect of the noise on the information transmission is significant which makes the channel capacity to become too low. On the other hand, for a large adiabatic temperature change, since the SNR is high, the effect of the noise on the information transmission is negligible; that is, the erroneous transmission probabilities p and q are too small.

The channel capacity C_{op} in bps changes with respect to the adiabatic temperature change ΔT_{ad} as shown in Fig. 7(b). Note that, since the signaling time T_s does not depend on ΔT_{ad}, the variations of the channel capacity in bit/use and bps with respect to ΔT_{ad} are the same. That is, for an adiabatic temperature change $\Delta T_{ad} = 0.1$ K, the channel capacity is $C_{op} = 28.9$ kbps and for an adiabatic temperature change $\Delta T_{ad} > 0.5$ K, the channel capacity saturates and becomes $C_{op} = 343.2$ kbps as illustrated in Fig. 7(b). Therefore, the channel capacity can be increased by increasing the adiabatic temperature change. However, since the channel capacity saturates as ΔT_{ad} increases, to minimize the effect of the temperature signals on the communication medium, the smallest ΔT_{ad} providing $C = 1.0$ bit/use can be used.

D. Effect of Thermal Diffusivity Constant

In the last analysis, we investigate the effect of the thermal diffusivity constant α of the communication medium on the SNR and the channel capacity of NHC. For this part of the analysis, the communication distance and the adiabatic temperature change are kept unchanged at $d = 500$ nm and $\Delta T_{ad} = 2$ K, respectively. The SNR variation with respect to the thermal diffusivity constant α is shown in Fig. 5(c). The SNR decreases with an increase in α. This is an expected result because as the thermal diffusivity constant increases, the average received power of the temperature signal $\overline{P}_s$ decreases, which can be seen in (25). Furthermore, substituting $T_s = 10t_{\max}$, $B = 2/T_s$, and (13) in (14) yields $\overline{P}_n = 2.4\alpha k_B T^2 d^{-2} C_V^{-1}$. Therefore, increasing α also increases the average received noise power $\overline{P}_n$. In addition, the SNR decreases abruptly when α is increased from 10^{-8} m^2/s to 4×10^{-6} m^2/s; then, it decreases slowly.

The channel capacity C in bit/use with respect to α is shown in Fig. 6(c). For low thermal diffusivity constants, since the SNR is too high as seen in Fig. 5(c), the effect of the noise on the information transmission is negligible; that is, the erroneous transmission probabilities p and q are too small. For example, for a thermal diffusivity constant $\alpha < 4 \times 10^{-6}$ m^2/s, the SNR > 10 dB and the channel capacity is very high, i.e., $C > 0.97$ bit/use. On the other hand, for a high thermal diffusivity constant, since the SNR is very low, the effect of the noise becomes significant and reduces the channel capacity.

The channel capacity C_{op} in bps changes with respect to the thermal diffusivity constant α as shown in Fig. 7(c). Note that, the variations of the channel capacity in bit/use and bps with respect to d are different because $C_{op} = 0.6\alpha C/d^2$ as found in Section V-A; that is C_{op} depends on α. Since C also depends on α, the effect of the α on C_{op} is not straightforward. The results show that increasing α from 10^{-8} m^2/s to 2×10^{-5} m^2/s increases the channel capacity C_{op} from 24.4 kbps to 19.2 Mbps. However, further increasing α decreases C_{op} because C becomes too low for high α values and its effect on C_{op} becomes significant. For instance, increasing α from 2×10^{-5} m^2/s to 10^{-4} m^2/s decreases C_{op} from 19.2 Mbps to 4.4 Mbps. According to the results, we can say that the channel capacity of NHC can reach very high communication rates by selecting a communication medium having an appropriate thermal diffusivity constant.

VI. Conclusion

In this paper, we propose NHC technique in which the heat transfer is used for the transmission of information at the nanoscale. The numerical analysis of NHC show that the channel capacity performance of NHC can reach very high rates over a long communication range compared with existing

nanocommunication methods in the literature. Furthermore, according to the results, the amplitude of the temperature signals does not need to be very high; thus, NHC can be used inside a living organism without harming living cells in the communication environment. Moreover, the channel capacity can be increased significantly by selecting a communication medium having an appropriate thermal diffusivity constant. As a result, NHC stands as a promising solution to nanoscale communication between nanomachines based on its channel capacity performance, advantages, and possible applications for the emerging field of nanonetworks.

REFERENCES

[1] S. Hiyama *et al.*, "Molecular communication," in *Proc. NSTI Nanotechnol.*, Anaheim, CA, USA, 2005, pp. 391–394.

[2] M. Gregori and I. F. Akyildiz, "A new nanonetwork architecture using flagellated bacteria and catalytic nanomotors," *IEEE J. Sel. Areas Commun.*, vol. 28, no. 4, pp. 612–619, May 2010.

[3] I. F. Akyildiz, F. Brunetti, and C. Blazquez, "Nanonetworks: A new communication paradigm," *Comput. Netw.*, vol. 52, no. 12, pp. 2260–2279, Aug. 2008.

[4] R. A. Freitas, *Nanomedicine, Vol. I: Basic Capabilities*. Austin, TX, USA: Landes Bioscience, 1999.

[5] M. Pierobon and I. F. Akyildiz, "A physical end-to-end model for molecular communication in nanonetworks," *IEEE J. Sel. Areas Commun.*, vol. 28, no. 4, pp. 602–611, May 2010.

[6] D. Kilinc and O. B. Akan, "Receiver design for molecular communication," *IEEE J. Sel. Areas Commun.*, vol. 31, no. 12, pp. 705–714, Dec. 2013.

[7] D. Kilinc and O. B. Akan, "An information theoretical analysis of nanoscale molecular gap junction communication channel between cardiomyocytes," *IEEE Trans. Nanotechnol.*, vol. 12, no. 2, pp. 129–136, Mar. 2013.

[8] J. B. Pendry, "Radiative exchange of heat between nanostructures," *J. Phys., Condens. Matter*, vol. 11, no. 35, pp. 6621–6633, Sep. 1999.

[9] J. B. Pendry, "Quantum limits to the flow of information and entropy," *J. Phys. A, Math. Gener.*, vol. 16, no. 10, pp. 2161–2171, Jul. 1983.

[10] E. Warburg, "Magnetische untersuchungen," *Ann. Phys. (Leipzig)*, vol. 249, no. 5, pp. 141–164, 1881.

[11] F. W. Sears, M. W. Zemansky, and H. D. Young, *University Physics*. Reading, MA, USA: Addison-Wesley, 1982.

[12] D. J. Bell *et al.*, "Manipulation of nanocoils for nanoelectromagnets," in *Proc. 5th IEEE Conf. Nanotechnol.*, Nagoya, Japan, 2005, pp. 303–306.

[13] H. Tohmyoh, H. Takeda, and M. Saka, "Fabrication of a free-standing pt micro-ring on an electrode chip as a small magnetic source," *J. Micromech. Microeng.*, vol. 19, no. 8, pp. 085013-1–085013-5, Aug. 2009.

[14] X. Q. Chen *et al.*, "Mechanics of a carbon nanocoil," *Nano Lett.*, vol. 3, no. 9, pp. 1299–1304, Sep. 2003.

[15] A. Nieuwoudt and Y. Massoud, "Understanding the impact of inductance in carbon nanotube bundles for VLSI interconnect using scalable modeling techniques," *IEEE Trans. Nanotechnol.*, vol. 5, no. 6, pp. 758–765, Nov. 2006.

[16] H. Li and K. Banerjee, "High-frequency analysis of carbon nanotube interconnects and implications for on-chip inductor design," *IEEE Trans. Electron Devices*, vol. 56, no. 10, pp. 2202–2214, Oct. 2009.

[17] P. L. McEuen and J. Y. Park, "Electron transport in single-walled carbon nanotubes," *Mater. Res. Soc. Bull.*, vol. 29, no. 4, pp. 272–275, Apr. 2004.

[18] F. Kreupl *et al.*, "Carbon nanotubes for interconnect applications," in *Proc. IEEE Int. Electron Devices Meet.*, 2004, pp. 683–686.

[19] V. K. Pecharsky and K. A. Gschneidner, Jr., "Giant magnetocaloric effect in $Gd_5(Si_2Ge_2)$," *Phys. Rev. Lett.*, vol. 78, no. 23, pp. 4494–4497, Jun. 1997.

[20] R. Hergt, R. Hiergeist *et al.*, "Maghemite nanoparticles with very AC-losses for application in RF-magnetic hyperthermia," *J. Magn. Magn. Mater.*, vol. 270, no. 3, pp. 345–357, Apr. 2004.

[21] Z. L. Wang, "Towards self-powered nanosystems: From nanogenerators to nanopiezotronics," *Adv. Funct. Mater.*, vol. 18, no. 22, pp. 3553–3567, 2008.

[22] S. Xu, B. J. Hansen, and Z. L. Wang, "Piezoelectric-nanowire-enabled power source for driving wireless microelectronics," *Nat. Commun.*, vol. 1, no. 7, pp. 1–5, Oct. 2010.

[23] M. Pierobon and I. F. Akyildiz, "Diffusion-based noise analysis for molecular communication in nanonetworks," *IEEE Trans. Signal Process.*, vol. 59, no. 6, pp. 2532–2547, Jun. 2011.

[24] B. S. Donahue and R. F. Abercrombie, "Free diffusion coefficient of ionic calcium in cytoplasm," *Cell Calcium*, vol. 8, no. 6, pp. 437–448, Dec. 1987.

[25] B. Atakan and O. Akan, "An information theoretical approach for molecular communication," in *Proc. 2nd Bionetics*, Dec. 2007, pp. 33–40.

[26] D. Demiray *et al.*, "DIRECT: A model for molecular communication nanonetworks based on discrete entities," *Nano Commun. Netw.*, vol. 4, no. 4, pp. 181–188, Dec. 2013.

[27] M. Pierobon and I. F. Akyildiz, "Noise analysis in ligand-binding reception for molecular communication in nanonetworks," *IEEE Trans. Signal Process.*, vol. 59, no. 9, pp. 4168–4182, Sep. 2011.

[28] M. Pierobon and I. F. Akyildiz, "Capacity of a diffusion-based molecular communication system with channel memory and molecular noise," *IEEE Trans. Inf. Theory*, vol. 59, no. 2, pp. 942–954, Feb. 2013.

[29] V. K. Pecharsky and K. A Gschneider, Jr., "Magnetocaloric effect and magnetic refrigeration," *J. Magn. Magn. Mater.*, vol. 200, no. 1–3, pp. 44–56, Oct. 1999.

[30] A. H. Morrish, *The Physical Principles of Magnetism*. Hoboken, NJ, USA: Wiley, 1965.

[31] T. Heimburg, *Thermal Biophysics of Membranes*. Weinheim, Germany: Wiley-VCH, 2007.

[32] L. E. Reichl, *A modern course in statistical physics*. Hoboken, NJ, USA: Wiley, 1980.

[33] A. O. Govorov *et al.*, "Gold nanoparticle ensembles as heaters and actuators: Melting and collective plasmon resonances," *Nanosc. Res. Lett.*, vol. 1, no. 1, pp. 84–90, Jun. 2006.

[34] B. H. Lavenda, *Statistical Physics: A Probabilistic Approach*. Hoboken, NJ, USA: Wiley, 1991.

[35] L. D. Landau and E. M. Lifshitz, *Statistical Physics (Course of Theoretical Physics Vol. 5)*. New York, NY, USA: Pergamon, 1980.

[36] H. Khlyap, *Physics and Technology of Semiconductor Thin Film-Based Active Elements and Devices*. Sharjah, United Arab Emirates: Bentham Science Publishers, 2009.

[37] J. Gallop and L. Hao, "Single crystal microwave dielectrics at low temperature: Losses and non-linearities," *J. Eur. Ceram. Soc.*, vol. 23, no. 14, pp. 2367–2373, 2003.

[38] W. Kim, R. Wang, and A. Majumdar, "Nanostructuring expands thermal limits," *Nano Today*, vol. 2, no. 1, pp. 40–47, Feb. 2007.

[39] L. W. Couch, *Digital and Analog Communication Systems*. Upper Saddle River, NJ, USA: Prentice-Hall, 2002.

[40] C. E. Shannon, "A mathematical theory of communication," *Bell Syst. Tech. J.*, vol. 27, pp. 379–423, Jul. 1948.

[41] A. K. Gupta and M. Gupta, "Synthesis and surface engineering of iron oxide nanoparticles for biomedical applications," *Biomaterials*, vol. 26, no. 18, pp. 3995–4021, Jun. 2005.

[42] J. Blumm and A. Lindemann, "Characterization of the thermophysical properties of molten polymers and liquids using the ash technique," *High Temperatures—High Pressures*, vol. 35/36, pp. 627–632, 2003.

Deniz Kilinc (S'12) received the B.Sc. degree in electrical and electronics engineering from Middle East Technical University, Ankara, Turkey, in 2011 and the M.Sc. degree in electrical and electronics engineering from Koc University, Istanbul, Turkey, in 2013. He is currently pursuing the Ph.D. degree in electrical and electronics engineering at Koc University, Istanbul. His current research interests include mathematical modeling and numerical analysis of biological systems.

Ozgur B. Akan (M'00–SM'07) received the Ph.D. degree in electrical and computer engineering from the Broadband and Wireless Networking Laboratory, School of Electrical and Computer Engineering, Georgia Institute of Technology Atlanta, GA, USA, in 2004. He is currently a Full Professor with the Department of Electrical and Electronics Engineering, Koc University and the Director of the Next-generation and Wireless Communications Laboratory. His current research interests are in wireless communications, nano-scale and molecular communications, and information theory. He is an Associate Editor for IEEE TRANSACTIONS ON COMMUNICATIONS and IEEE TRANSACTIONS ON VEHICULAR TECHNOLOGY, Editor for International Journal of Communication Systems (Wiley), Nano Communication Networks Journal (Elsevier), and European Transactions on Telecommunications (Wiley).